Vertical and lateral ordering of Ge islands grown on Si(001): theory and experiments

2007 J. Phys.: Condens. Matter 19 225001

(http://iopscience.iop.org/0953-8984/19/22/225001)

IOP PUBLISHING JOURNAL OF PHYSICS: CONDENSED MATTER

J. Phys.: Condens. Matter **19** (2007) 225001 (22pp) doi:10.1088/0953-8984/19/22/225001

Vertical and lateral ordering of Ge islands grown on Si(001): theory and experiments

F Montalenti[1], A Marzegalli[1], G Capellini[2], M De Seta[2] and Leo Miglio[1]

[1] L-NESS and Dipartimento di Scienza dei Materiali della Università degli Studi di Milano-Bicocca, Via Cozzi 53, I-20125 Milano, Italy
[2] Dipartimento di Fisica E. Amaldi, Università Roma Tre, Via della Vasca Navale 84, I-00146 Roma, Italy

E-mail: francesco.montalenti@unimib.it

Received 29 May 2006
Published 14 May 2007
Online at stacks.iop.org/JPhysCM/19/225001

Abstract

A set of recent results concerning lateral and vertical ordering of Ge islands grown on Si(001) is reviewed. Experimental data generated by chemical vapour deposition and analysed by atomic force microscopy and photoelectron spectroscopy are compared with computer simulations and modelling based on atomistic approaches and continuum theory. In particular, we show that it is possible to probe experimentally the detailed strain field generated by buried Ge islands at the surface of the Si capping layer. The observed arrangement of small Ge islands grown over the capping layer is demonstrated to be very close to the one predicted by a simple model where the local chemical potential is inferred from the strain field at the atomic scale, as given by Tersoff-potential molecular dynamics simulations. Moreover, we review recent experimental evidence for lateral ordering, triggered by partial Si capping, in the first layer of Ge islands on Si(001). Theoretical support is given by showing that when two islands lie in close proximity the elastic field is likely to generate a flow of atoms leading to an effective gliding motion along opposite directions of both islands, eventually stopped by the presence of further neighbouring islands.

(Some figures in this article are in colour only in the electronic version)

1. Introduction

It is often difficult to point out which paper determined the success of a popular scientific research field, or who first unravelled the key physical phenomenon leading to subsequent key advancements. Concerning the study of three-dimensional (3D) Ge islands on Si(001), evidence of their formation was already reported in the early 1970s (see, e.g. [1, 2]). However, the key experimental discoveries which led to the development of the field as we intend it nowadays can be probably attributed to the papers of Eaglesham and Cerullo [3] and of Mo *et al* [4]. Exploiting advanced characterization techniques such as transmission electron microscopy

(TEM) and scanning tunnelling microscopy (STM), these authors showed that nanometre-scale Ge islands could be grown on Si(001) without introducing misfit dislocations either in the island or in the substrate. Moreover, it was possible to characterize at the atomic scale the typical shape of the Ge islands. Both the lack of extended defects and the actual size of the islands soon appeared to be key in determining possible applications of technological relevance in the development of future nanodevices. In this respect, the possibility of exploiting the already well developed silicon technology was surely an additional bonus to promote further investigation of Ge/Si systems.

While in [4] Ge islands appeared as characterized by {105} facets, corresponding to a height to base aspect ratio of $\sim$0.1, further studies [5–7] clarified that, above a certain volume, the shape of the islands changes dramatically, evolving from platelets to shallow {105} pyramids (or, depending on the growth temperature, {105} rectangular huts) to multifaceted domes of roughly double aspect ratio. Typical samples containing several Ge islands revealed a clear bimodal distribution [6] of large domes and smaller pyramids. The pyramid-to-dome transition has been the subject of several studies. A thermodynamic model, able to recover the main experimental findings, was proposed [8, 9], showing that the shape transition corresponds to a discontinuity in the atoms' chemical potential. More recently, the detailed atomic pathway leading to the transformation from pyramid to domes was unravelled, on the basis of high-resolution STM images and theoretical modelling [10] taking into account the dependence of the chemical potential on the position within the island, regions closer to the apex being favoured due to the stronger lattice-parameter relaxation (see also [11, 12]). A very nice agreement between theoretical modelling and experimental data on the shape transformation has been reported [10, 13, 14]. Interestingly, when Ge domes are capped with Si, an inverse transformation takes place [15, 16], buried islands displaying again a (truncated, see sections 4 and 5) pyramidal shape.

Understanding the typical shape and size is only a starting point in order to build up a general understanding of Ge islands on silicon. For application purposes, it is of utmost interest to prepare spatially ordered arrays of islands, both in structures containing a single layer and in multilayered arrays where Ge islands are deposited alternately with silicon capping layers (CL). The possibility of exploiting self-organization was soon individuated as a fascinating route. Ge islands, when capped, generate a tensile strain field above them, thus lowering the chemical potential of further Ge atoms deposited on the capping layer. As shown by Tersoff *et al* (TTL) [17], a simple elastic-theory based model, where embedded islands are studied as point-like elastic dipoles, is able to predict that in a multilayered structure the islands tend to reach both spatial (vertical and lateral) and size ordering, in spite of the tendency to nucleate randomly in the first layer. In the same paper, comparison with experiments yielded a satisfactory qualitative agreement. While the TTL model was a real breakthrough, clearly suggesting and justifying the possibility of reaching size and space ordering by pure self-organization, it was admittedly not meant to actually capture the whole complexity of the growth process. More recently, much new information has been collected, sometimes leading to significant changes in the interpretation of ordering of Ge islands on Si(001). It is the aim of the present paper to review our recent work dealing with a unified theoretical and experimental picture of some key aspects of ordering in both single-layer Ge islands on Si(001), and in multilayered structures. In several cases, the discussion of the results is significantly extended with respect to the original references. While the investigation of multilayered structures should logically follow the understanding of single-layer organization, the physics of the latter is more complex, so that we shall first discuss results for vertical alignment, and only after analyse lateral interactions in uncapped and partially capped Ge islands. The interested reader can find more general reviews of island formation, growth, and self-organization in Ge/Si systems in [18–24].

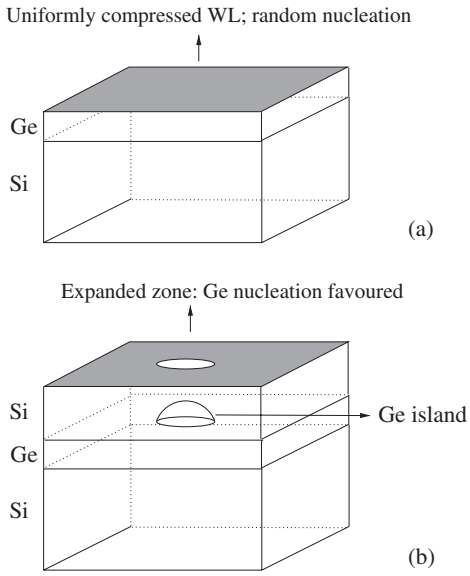

Figure 1. (a) Schematic representation of a Ge WL on Si(001). The WL is uniformly strained, so that island nucleation at the WL surface is random. (b) If Ge islands are capped with Si, at the CL surface the strain is not uniform. When additional Ge atoms are added, an energetically favoured region is found above the embedded island.

2. A simple approach to strain-induced ordering

The lattice parameter of Ge is ∼4% larger than the Si one. As a result, Ge atoms deposited on Si feel a strong biaxial compressive stress, which causes the well known Stranski–Krastanov growth mode characterized by the formation of a thin (3–4 ML) Ge wetting layer (WL) preceding 3D island formation. Since the WL is uniformly strained, initial island positioning is random (see figure 1(a)). Si complete capping of Ge islands generates a non-uniform strain distribution at the CL surface. The island, indeed, exerts a tensile action, which propagates within the CL, resulting in a strain modulation at its surface. In particular, the region above the buried island is characterized by an effective in-plane lattice parameter which is expanded with respect to Si and less compressed with respect to Ge when compared with the ∼4% value of the WL. Being closer to their ideal lattice parameter, critical nuclei of Ge atoms forming in this region will be more stable, facilitating the formation of islands (see figure 1(b)). While this is only a qualitative picture of the situation, it is possible to estimate the actual strain distribution at the CL surface. To a first approximation, using continuum elasticity theory, and treating the buried island as a force dipole, the trace ε of the strain tensor at the CL surface can be computed analytically [17, 25] by using the simple relation

$$\varepsilon = CV(r^2 + H^2)^{(-3/2)}\left(1 - \frac{3H^2}{r^2 + H^2}\right). \tag{1}$$

Here H is the thickness of the CL, computed from the island basis, $r^2 = x^2 + y^2$ is the distance from the island in the surface plane, V is the dot volume, and C is determined by the elastic constants [26]. If more than one island is present inside the CL, then the total strain at the CL surface can be computed by simply summing up the different contributions. While equation (1) describes a system in $(2 + 1)$ dimensions, the key physics of the alignment process can be inferred by a simpler model where the surface of the CL is one dimensional (set $r^2 = x^2$ in

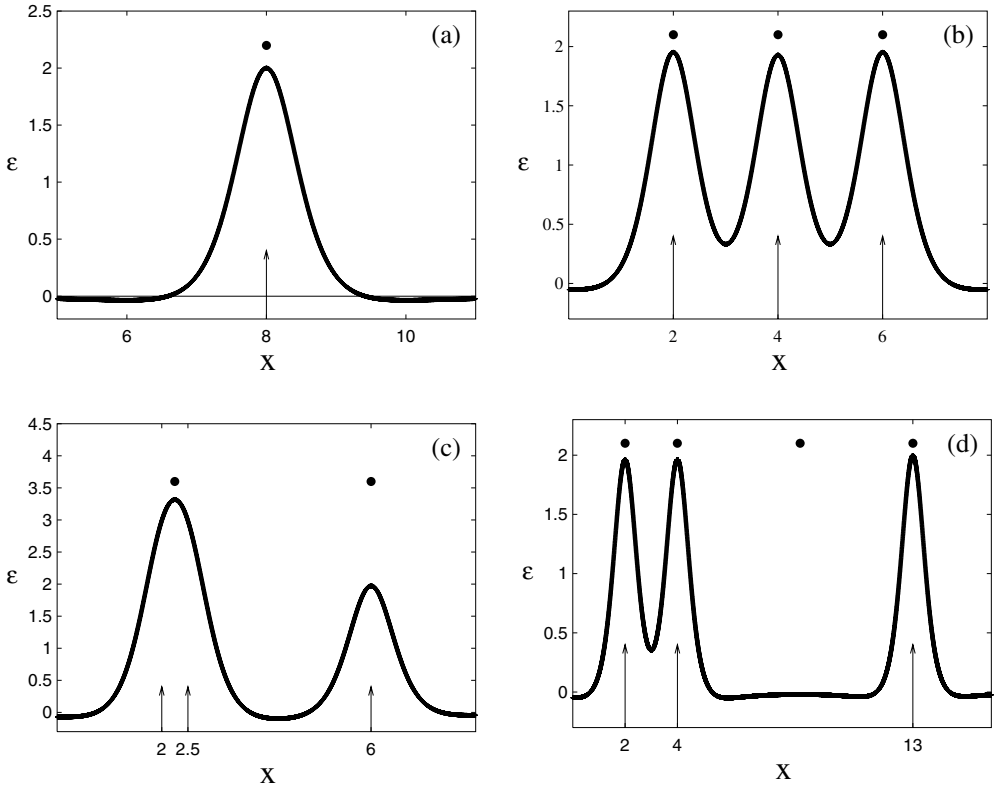

Figure 2. Trace of the total strain field at the CL surface due to one (panel (a)) or three (panels (b), (c), and (d)) point-like islands, as given by equation (1), using $C = -1$, $H = 1$, and measuring x in units of H and ε in units of $[CH^{-3}]$. In each panel, arrows at the bottom represent the island position, while full circles in the upper part indicate favoured nucleation sites for the next layer of islands. (a) Isolated island located at $x = 8$. Notice that, away from the maximum, the trace of the strain field becomes slightly negative, indicating a small compressive action. (b) The islands are located at $x = 2, 4, 6$; there are three nucleation sites, vertically aligned with the islands. (c) The islands are located at $x = 2, 2.5, 6$; there are only two nucleation sites, one between two islands, the other vertically aligned with the third one. (d) The islands are located at $x = 2, 4, 13$; there are four nucleation sites, one (vertically aligned) for each island, plus a fourth one located between the more distant islands.

equation (1)). The typical strain field caused by an isolated island is shown in figure 2(a). Obviously, the preferred nucleation site (indicated by a full circle) is vertically aligned with the island. As a more significant example, we now consider three islands located at different positions. Following [17], we shall assume that each local maximum of ε corresponds to the location of the centre of mass of a new Ge island deposited on the CL[3]. Panel (b) represents perfect one-to-one vertical alignment. If two capped islands are very close, however, the superposition of the strain fields cancels one nucleation site. This situation is represented in panel (c). On the other side, if one island is very distant from the others, a new maximum appears, so that four nucleation sites (three vertically aligned plus the additional one) are now present (panel (d)). The beauty of the TTL model is that, despite being extremely simple, it is

[3] In [17] a negative-strain convention is used, so that the curves appear the negative of ours, and nucleation is signalled at local minima. Since in the following, however, we shall often talk about tensile (positive) strain, here we prefer not to follow that convention.

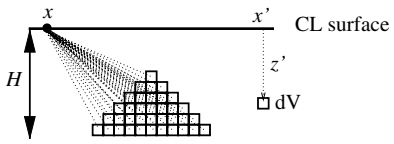

Figure 3. Within continuum elasticity theory, the trace of the strain tensor at the surface of the CL produced by a buried island can be computed by dividing the island into infinitesimal volumes dV, by treating each of them as elastic dipoles, and by summing each contribution through an integration procedure. Here, a simple two-dimensional representation is given; x represents the point of the CL surface where the strain is computed, while (x', z') are the horizontal and vertical coordinates, respectively, of an infinitesimal portion of the island. The width H of the CL is computed from the island base.

able to foresee a very intriguing behaviour. As suggested by the example of figure 2, it is the superposition of the strain fields to induce lateral ordering in the islands. While a single layer of sandwiched islands is not sufficient, by iterating the procedure (see [17] for further details, in particular for what concerns the attribution of the individual volumes in the new layer of islands) the average distance between the islands tends to approach a constant value. Under these conditions lateral and vertical ordering are achieved at the same time. Moreover, the size distribution gets very narrow [17]. While this model captures the essential features of the observed self-organization process in multilayered SiGe structures, there are several aspects which are oversimplified. In the following section we shall relax the point-like hypothesis, and compute the strain field induced in the CL by realistically shaped 3D islands by atomistic simulations.

3. Beyond point-like islands

While equation (1) has been broadly used to provide qualitative estimates of the strain field, recent theoretical results have clearly shown that, under typical experimental conditions in terms of island size and CL thickness, a more refined approach is needed, since the actual shape of the island plays an important role in determining ε. It is worth emphasizing that it is possible to capture the main features of the shape-dependent strain field generated at the CL surface by integrating the dipole formula over the volume occupied by the dot, as schematically represented in figure 3.

The trace of the total strain $\varepsilon_{\mathrm{tot}}$ at the position $(x, y, z = 0)$ (CL surface) is then given by [26]

$$\varepsilon_{\mathrm{tot}}(x, y) = \int_V \varepsilon(x - x', y - y', z')\, \mathrm{d}x'\, \mathrm{d}y'\, \mathrm{d}z', \tag{2}$$

where $\varepsilon(x', y', z')$ is obtained from equation (1) by setting $r^2 = (x-x')^2+(y-y')^2+(z')^2$, with (x', y', z') representing points within the volume V of the island. Applications of equation (2) can be found in recent papers [26, 27], showing a strong dependence of the strain field on the island geometry.

Here we have briefly described the method used in [26, 27] since it corresponds to the most immediate extension of equation (1) which we used as an example of a simple treatment of the problem. It must be pointed out, however, that several alternative methods exist, yielding reliable estimates of the strain field induced by an embedded island. For example, finite-element calculations solving the equations determining the equilibrium condition for a linear elastic body [28, 29] can be used. Alternatively, one can accept a further degree of complexity and a heavier computational demand, by using atomistic simulations based on semiempirical

potentials (first principle calculations are out of question, since a simulation cell of several nanometres is needed). Indeed, the first evidence on the important deviations from the point-like dipole formula have been first reported by Makeev and Madhukar [30], who carried out extensive atomistic simulations of pyramidal islands. While in [26] it was explicitly shown that the simpler and faster approach based on equation (2) was able to recover the main features reported by Makeev and Madhukar, using an atomistic approach remains highly appealing, yielding information on the deformation fields at the atomic scale, being able to consider deviations from linearity, and allowing us in principle to consider the effect of localized or extended defects (e.g., dislocations [31]), which are hard to include in a consistent continuum-theory investigation. Let us now describe how we obtained a detailed description of the strain field by using classical molecular dynamics (MD) simulations.

4. Atomistic simulations of the strain field

We have simulated the deformation field induced by an isolated, Si-capped Ge island of different shapes on Si(001), by using classical MD simulations. The Si–Si and Si–Ge interaction was described by the Tersoff potential [32] which gives a nice description of the elastic properties of both Si and Ge. While we shall not describe the general form of the potential, we recall that its many-body form allows one to take into account the covalent nature of the bonds in diamond-like structures. In the past, such potential has also been shown to yield reliable results in predicting critical quantities such as the energetic ordering of complex reconstructions (see, e.g. [33]). The Tersoff potential tends to lose its validity when strong bond undercoordination is present. While this may cause problems when attempting to estimate kinetic barriers [34], in the present context we shall simply evaluate distortions of the diamond lattice, so that we expect our approach to be rather accurate and reliable.

The simulation cell that we used is characterized by an extension of 33 nm in both [100] (x) and [010] (y) directions, periodic boundary conditions (PBCs) being applied in both x and y. In the [001] (z) direction, we considered a substrate made of 5.4 nm of Si atoms, covered by three monolayers (ML) of a Ge WL supporting a Ge(105) pyramid of base $L = 22$ nm truncated at its half-height (and thus delimited by a mesa in its upper region), buried in an $H = 2.5$ nm Si CL. Simulations were also repeated for a thicker ($H = 5.4$ nm) CL. The truncated-pyramid shape of the Ge island reproduces, in terms of aspect ratio and presence of an upper mesa, the typical geometry of buried islands in SiGe multilayered structures, as revealed by transmission electron microscopy in [35]. A further discussion concerning the actual shape of real islands will be presented in section 5. A good idea of the simulation geometry can be inferred directly from the strain maps of figure 4. Some of the results discussed in the following were also obtained with slightly different simulation cells. In such cases, the actual size is always specified.

While the Ge/Si system was initially forced at the Si lattice positions, a long relaxation cycle was used in order to find the minimum-energy configuration. In particular, we have used a thermal cycle, heating the system from 0 to 400 K, then cooling it back to 0 K, and finally performing quenched molecular dynamics. The time step was set to 2 fs. During simulated annealing and quenched MD, we allowed all of the atoms to relax, with the exception of the four bottom layers of the Si substrate, which were kept frozen to bulk positions. After the system reached its minimum-energy value, we computed the strain tensor $\epsilon_{\alpha,\beta}$ with atomic resolution by evaluating the transformation matrix between the ideal and the actual, distorted vectors connecting each atom to its four nearest neighbours [38]. The ϵ_{xx} component is plotted in figure 4 (ϵ_{yy} displaying an analogous behaviour), where a grey (colour online) scale is used to represent ϵ_{xx} along a y/z section of the simulation cell halving the island. Since here we are mostly interested in the tensile action exerted at the CL surface, we have chosen the scale so

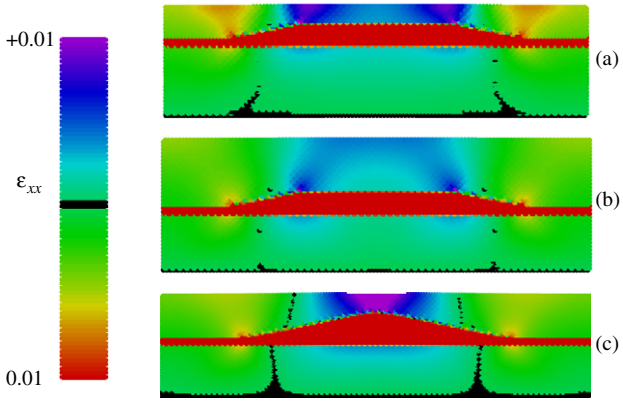

Figure 4. Plots of the ϵ_{xx} component of the strain tensor. (a) Truncated {105} pyramid; thin ($H = 2.5$ nm) CL. (b) Truncated {105} pyramid; thicker ($H = 5.4$ nm) CL. (c) Complete {105} pyramid. While the data reported in panels (a) and (b) exactly correspond to those displayed in figure 1 of [36], with the cell size specified in section 4, the complete pyramid data were taken from a different set of simulations [37], where the base length was set to 27 nm, $H = 4.6$ nm, while the extension of the cell in x and y was 44 nm (the same number of Si substrate layers was used). Black dots are just an artifact of our plotting code: they correspond to *exactly* zero-strain regions.

that strongly (more than 1%) compressed regions are uniformly shaded. As a result, the whole embedded island and the WL are easily recognized in the figure. Let us start analyzing panel (a), where results are shown for the thinner ($H = 2.5$ nm) CL. Quite evidently, from both the lower (intersection between the {105} facets and the WL) and the upper (intersection between the {105} facets and the top flat mesa) edges, a strong strain field originates. Similarly to what happens when a step is present on a compressed surface, the upper edge causes a tensile action, while the lower acts as a compression centre. The free surface (setting the zero-stress condition at its boundary [28]) influences the actual shape of the deformation field. The final result is that the most expanded regions at the CL surface lie roughly above the mesa boundaries. If a thicker CL is considered (panel (b), where $H = 5.4$ nm), the top-expansion lines bend, so that the maximum expansion region is now broadly distributed above the centre of the mesa. The above described migration of the most expanded region from side to centre is directly related to the presence of the upper (001) facet, and, in fact, it has also been observed for rectangular-prism shaped islands [27]. As is natural to foresee, at large enough distances the details of the island geometry tend to be less effective in influencing the strain field. As a consequence, the action of a truncated island becomes qualitatively similar (central most expanded region) to what one would obtain for a complete {105} pyramid, shown in panel (c).

Following [17], the CL surface regions of maximum tensile strain are the best candidates to become nucleation sites if further Ge is deposited over the free surface. Let us now try to expand this concept, trying to predict an actual island arrangement. With this goal, we define a local chemical potential $\mu(x, y)$ reflecting the energy variations with respect to the perfect bulk, due to elastic effects. In practice, we start by considering the in-plane strain

$$\epsilon(x, y) = 1/2 \times (\epsilon_{xx}(x, y) + \epsilon_{yy}(x, y)), \tag{3}$$

at the (x, y) position of the CL surface, as given by our MD simulations. Such strain is relative to the Si lattice parameter. After transforming it into the corresponding strain relative to Ge, we compute the energy per atom of Ge tetragonally strained at the local value of $\epsilon(x, y)$, i.e. we consider a bulk forced in the (x, y) directions to the local in-plane strain, while able to relax in z until it reaches a minimum energy condition. Notice that, following our definition, $\mu(x, y)$

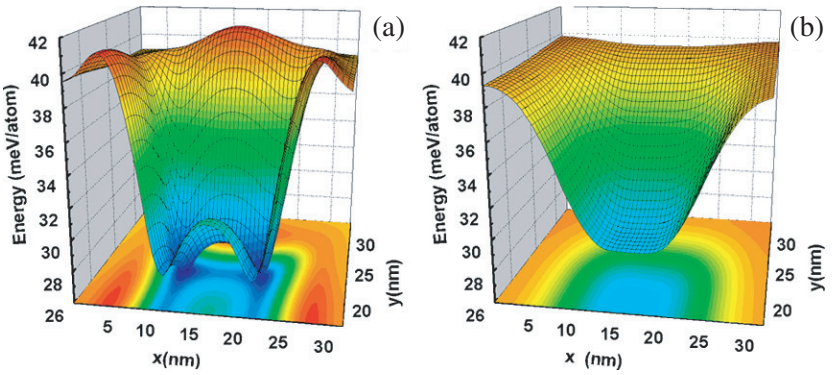

Figure 5. Section of the chemical potential $\mu(x, y)$ at the CL surface. Panel (a) corresponds to the thinner CL ($H = 2.5$ nm) (see figure 4(a) for the corresponding ϵ_{xx} map), while panel (b) reports the results for $H = 5.4$ nm (see also figure 4(b)). In both cases the total curve is symmetric with respect to the $y = 16.5$ nm axis. The figure is reprinted with permission from [36]. Copyright 2005, American Institute of Physics.

is not meant to represent the energy of an additional Ge atom deposited directly over the Si CL surface. Indeed, due to the strength of the Si–Ge bond with respect to the Ge–Ge one and to the lower Ge surface energy, it appears reasonable to predict that Ge would preferentially wet the whole CL surface before forming the islands (an experimental confirmation of this fact is given, e.g., in [39]). Once one or a few Ge layers are formed at the CL surface, then our $\mu(x, y)$ becomes meaningful for the energy per atom gained by the system by placing a Ge atom in (x, y). Results for $H = 2.5$ and 5.4 nm are displayed in figure 5. The observations made in commenting on figure 4 now become even clearer. For the thinner CL (figure 5 a), the region above the centre of the embedded dot (the island lower base is located between $x \sim 5.5$ and $x \sim 27.5$ nm) corresponds to a maximum in the chemical potential, while four symmetric minima are located close to the walls which border the region directly influenced by the tensile action. The shape of $\mu(x, y)$ changes dramatically by increasing the extension of the CL to $H = 5.4$ nm: in figure 5(b) the curve is much smoother, and the minimum-energy condition is reached at the centre. In order to exploit the single-atom chemical potential of figure 5 to predict actual island arrangement, we make use of a very simple model. We define an island as a covered CL portion, which, for simplicity, is taken as a square (with sides along the [100] and [010] directions). The energy of the island is then defined as the sum of $\mu(x, y)$ over all the atoms belonging to the covered region. If N such two-dimensional islands are present at the same time, we seek the minimum total energy (sum of the individual islands' energies). In doing so, we let each island be free to move in (x, y), but we do not allow for any coalescence, placing infinite repulsive walls for island–island distances smaller than 1 nm. A simple iteration of steepest-descent steps and initial position randomization was sufficient to find the optimized position. The final configurations for $N = 8$ (the number is suggested by the experiment, see section 5) and $L \sim 3$ nm are shown in figure 6(a) for $H = 2.5$ nm and in figure 6(b) for $H = 5.4$ nm. It is evident that for the thin CL the small islands are able to sample the changes in chemical potential within the well, so that the central region, corresponding to the local maximum in $\mu(x, y)$, remains void. In the thicker CL case, instead, the cluster of small islands is more compact and completely occupies the region directly above the mesa. The behaviour is so qualitatively different that one can hope to find experimental evidence that our simple model, based on pure local-thermodynamics arguments, has predictive power. Before attempting to compare with experiments, however, some observations must be made. First, we

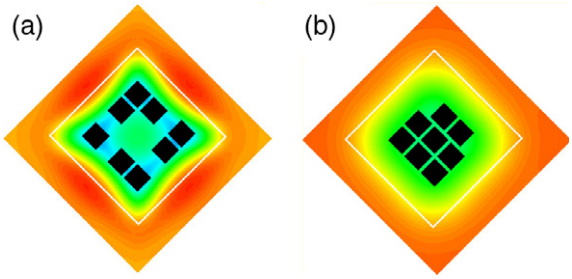

Figure 6. Minimum-energy configuration for eight islands of base $L \sim 3$ nm placed over the 2.5 nm CL (panel (a)) and over the 5.4 nm CL (panel (b)). The white box indicates the extension of the island base. Shades correspond to the scale of figure 5. The figure is reprinted with permission from [36]. Copyright 2005, American Institute of Physics.

notice that, due to computational limitations, the bases of our buried islands are roughly ten times smaller than real ones [35, 39]. On the other hand, the typical CL thickness is also about ten times smaller. In this sense, if our simulation cell is large enough to enter the self-similar behaviour range, then a direct comparison is possible. We have actually checked this issue by running a second set of simulations where both the island basis and the CL thickness was increased by a factor of 1.5. Strain maps compared very well with those reported in figure 4. The second important point deals with the dimensions of the second layer of islands. Obviously, if these islands have the same dimensions as the buried one, differences in the local chemical potential within the well will be insignificant, leading to vertical, one to one alignment (at least if the capped island does not have close neighbours, see section 2). Thus, if one wishes to use the upper-layer islands as a probe for the CL-surface strain field, such islands must be much smaller than the underlying ones. From figure 6(a), for example, it is quite evident that islands of double size with respect to the one represented would be forced to occupy the central region, in order to avoid climbing on the very steep lateral walls of the potential well. Let us now describe how it was possible to actually achieve this goal experimentally.

5. Growing small clusters of islands at the CL surface by CVD

All the samples described in this study have been deposited on Si(001) substrates in an ultra-high vacuum chemical vapour deposition reactor whose base pressure was in the low 10^{-10} Torr range. The deposition was performed using high purity silane and germane without carrier gas. Typical reacting gas pressure during the growth was in the range 10^{-4}–10^{-3} Torr. The substrate temperature has been measured by means of an infrared pyrometer with an accuracy of $\pm 5\,^{\circ}$C.

As we shall describe in detail in the next section, the exposure of Ge/Si islands to a flux of silicon atoms during the capping procedure results in an island shape change and in a size enlargement. The main reason for this transformation is the incorporation of the impinging Si atoms into the island and the consequent Si–Ge intermixing. In figure 7 we present a cross-section TEM image obtained on a Ge/Si island multi-layer deposited having the last island layer left uncapped. While all the island layers have been grown in the same deposition conditions, the multi-faceted dome in the topmost layer is characterized by a higher aspect ratio and a smaller base with respect to the buried truncated pyramids. The latter have a typical base width of 220 nm and a height of about 10 nm.

From the previous section of this paper we can evaluate that the strain field at the surface generated by buried islands of this size has a lateral extension of about 250–300 nm. Therefore, in order to sample a strain field of this size we need to deposit islands having width in the 25–

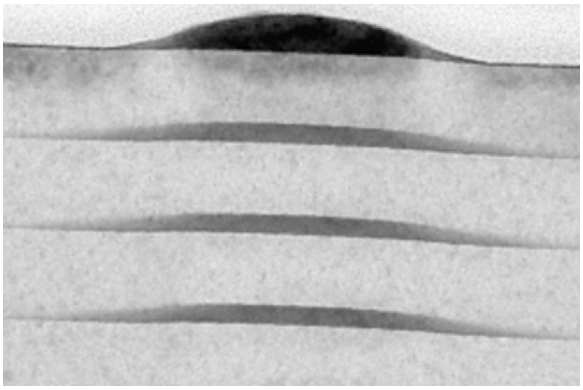

Figure 7. Cross-sectional TEM image of a multilayer grown at 750 °C. The buried islands are the evolution of the multifaceted dome visible in the topmost layer after capping with a 65 nm thick silicon layer. The flattened buried islands have typical base width $b = 220$ nm and height $h = 10$ nm while the uncapped dome is characterized by $b = 180$ nm and $h = 35$ nm.

30 nm range. To this purpose we prepared the samples using the following procedure. First, a tenfold island multilayer was deposited in order to improve the island shape and size uniformity by exploiting the island–island strain interaction along the growth direction. This allows one to have an ensemble of identical *stressors* under the silicon cap layer [35]. This island layer was then buried under cap-layers of different thicknesses in order to vary the strain field modulation at the free surface as calculated in section 4. The entire stack was deposited at 750 °C. In order to obtain islands having size smaller than the strain field lateral extension, we deposited the island over the strain-modulated silicon surface at 600 °C. We demonstrated how the island size can be reduced by reducing the extent of the intermixing phenomenon [40, 41]. As a matter of fact, the enlargement of the width of the critical base for the formation of three-dimensional Ge/Si islands observed upon increasing the deposition temperature is mainly due to a thermally enhanced intermixing phenomenon that enriches the islands of silicon and offers an alternative way to accommodate the heteroepitaxial strain [40, 41]. This phenomenon can be hindered by using a lower deposition temperature as can be understood from figure 8, where we show the relationship between the critical base as a function of the deposition temperature for an island layer having the same equivalent thickness and deposited at similar growth rate. A fine tuning of the deposited material allowed us to obtain small islands having pyramidal shape and size of about 30 nm [39].

Atomic force microscope (AFM) images of the typical island arrangement in clusters are displayed in figure 9 for a thin (∼25 nm; see panel (b)) and a thick CL (∼54 nm; panel (c)), respectively. By comparing these results with the theoretical ones of figure 6, a close correspondence is immediately seen. Both theory and experiments predict the presence of a void central region for thin CL having a width of about $1/10$ of the buried island base, while a close-packed cluster located in the region right over the island top is observed for the thick CL.

It is important to emphasize that the agreement between experiments and theory is not only qualitative. In figure 10 we report the value of the island–cluster diameter Δ_{Exp} as a function of the deposition time for sample deposited on a ∼25 nm thick CL (circles) and on a ∼54 nm thick CL (squares). The cluster diameter Δ_{Exp} has been defined as the diameter of a circle having a surface equivalent to that delimited by the perimeter that includes all the islands belonging to the cluster itself. In order to understand the cluster growth dynamics, we

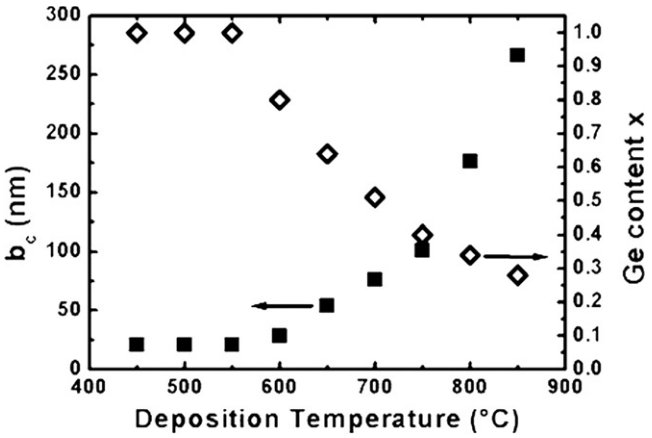

Figure 8. Critical base for three-dimensional transition (squares) and average composition of the island layer (diamond) as a function of the deposition temperature, as measured in [40]. Data were collected from samples deposited at the same growth rate of 1.5 nm min^{-1}.

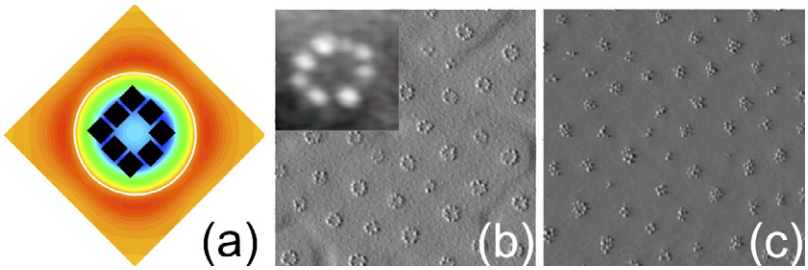

Figure 9. (a) Minimum-energy configuration for eight islands of base $L = 3$ nm placed over an island having a truncated-cone shape, buried under a 2.5 nm CL. The white circle indicates the extension of the island base. Shades correspond to the scale of figure 5. (b) $2 \times 2\ \mu\text{m}^2$ AFM images displayed in differential mode of Ge-island clusters deposited on an $H = 25$ nm thick CL. In the inset we show a cluster made of eight individual islands (using a grey scale reflecting the island height). The image sides are aligned along the [110]-equivalent direction. (c) as in (b), but for $H \sim 54$ nm. The figure is reprinted with permission from [36]. Copyright 2005, American Institute of Physics.

have measured the base width b of the individual islands as a function of the deposition time (about 2000 islands were taken into account for each sample). From figure 6 we can observe that, in the thinner cap-layer samples, the islands tend to nucleate across the contour-plot line joining the four minima of $\mu(x; y)$, i.e. in a region having a theoretically estimated diameter $\Delta_{\text{Th}} = 120$ nm (if we take into account the $10\times$ scaling factor from simulation to experiments). After the nucleation the germanium atoms incoming from the supplied gas are incorporated into the existing individual islands belonging to the cluster, increasing their average size as sketched in the right panel of figure 10. The average cluster diameter will therefore increase with the deposited material following the relationship $\Delta(t) = \Delta_{\text{Th}} + b_m(t)$, where b_m is the average base width of an individual island. The values predicted by this relationship as a function of the sample deposition time are reported in figure 10. The nice agreement between the theoretical predictions and the measured cluster diameter is strong evidence for the hypothesis of nucleation and growth dynamics we proposed.

The behaviour of Δ_{Exp} in the thick CL limit is also in agreement with the nucleation mechanism we obtained in section 5. As a matter of fact, the cluster diameter at the early stage

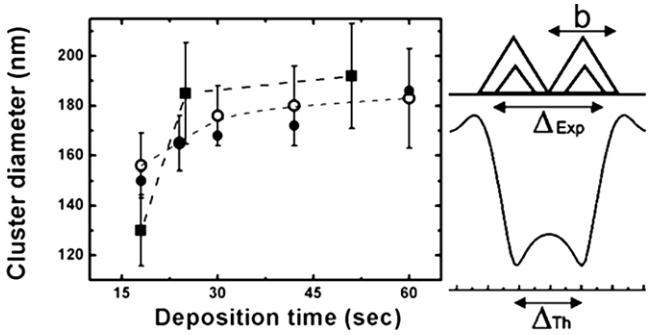

Figure 10. Evolution with the island deposition time of the cluster diameter Δ_{Exp} measured on ∼25 nm thick (filled circles) samples and on ∼54 nm thick CL samples (filled squares with a dashed line as a guide for the eye). The corresponding diameter evolution for the 25 nm case, as predicted by the formula $\Delta(t) = \Delta_{\mathrm{Th}} + b_m(t)$ (see the text), is shown by empty circles with a dashed line as a guide for the eye. The error bars in $\Delta(t)$ are given by the standard deviation of the $b_m(t)$ distribution measured over the samples.

of nucleation (we assume here the same growth rate on both experimental series) is smaller here than in the thin CL case. This is not surprising. The islands nucleate in the central region of the potential well and, as the deposition proceeds, new islands nucleate at the boundary of the cluster until a *saturation* value of the cluster diameter is reached. This value corresponds to the lateral extension of the tensile strain field at the surface. Above this limit nucleation in the cluster is not favoured anymore and we can observe the loss of the growth selectivity as described in [39].

So far, we have only analysed successful comparisons between theory and experiments. Refining the level of analysis, however, one can find a small discrepancy in the island location when comparing figure 6(a) with figure 9(b): the clusters of small Ge islands tend to have a more circular symmetry with respect to those obtained from our simulations. This is probably due to the actual geometry of the mesas of the buried islands. High-resolution scanning tunnelling microscope images [15] have indeed shown that Ge islands partially capped with Si can display a geometry more complex and multifaceted than a truncated pyramid. We therefore replaced the pyramidal shape in our model with the limiting case of a truncated cone. In figure 9(a) we reported the resulting cluster configuration obtained for the thin CL case with a buried truncated cone. As expected, the main features revealed by figure 6(a) are conserved (empty central region), while the more rounded symmetry of the experimental clusters is better accounted for. The close agreement between the island arrangement observed experimentally with the one predicted by our model (see figure 9(a)), suggests that, in our sample also, the buried Ge islands have a top facet having a more rounded boundary geometry.

6. Lateral ordering of islands at the first layer

As we discussed in section 2, the strain field generated at the CL surface by buried islands guarantees a progressive lateral ordering in multilayered structures. Following the TTL model, once islands are formed with a given spatial distribution, they play a rather passive, although important, role. Simply, once capped, they act as inclusions deforming the CL, and driving selective nucleation. In reality, the capping procedure deeply modifies the islands, changing their shape (domes transform back into pyramidal-like islands [15]) and influencing the degree of Si intermixing (for a detailed study, see [16]). Let us now show that capping, under suitable experimental conditions, is already able to promote lateral ordering in the first layer.

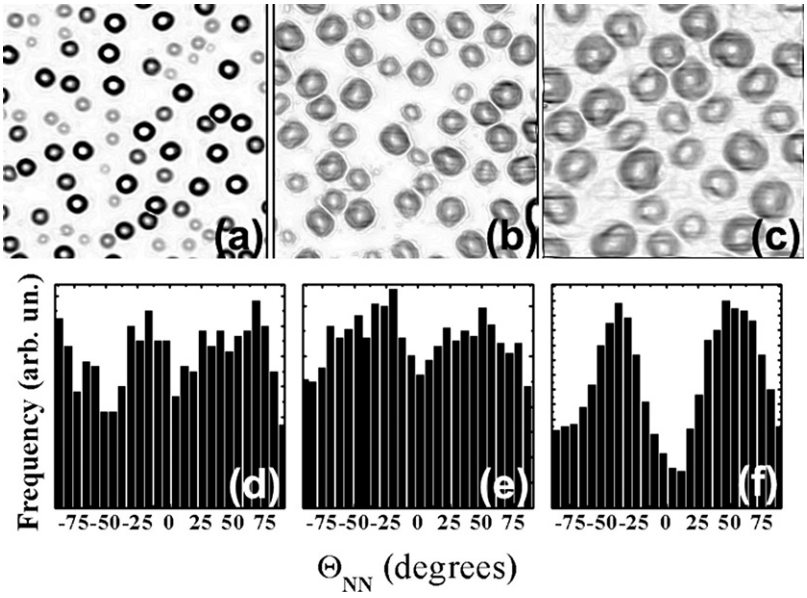

Figure 11. $2 \times 2\ \mu m^2$ AFM images displayed in differential mode of a Ge island layer deposited at 750 °C and having an equivalent thickness of 1.5 nm covered by a (a) 0 nm, (b) 1.8 nm, and (c) 6 nm thick silicon cap layer. Image sides are oriented along [110] directions. In panels (d)–(f) we display the corresponding angular distribution of the four nearest neighbours.

In figure 11 we display the evolution of the surface morphology of samples obtained depositing a different Si coverage on top of a nominally identical Ge island layer ((a) $\theta_{Si} = 0$, (b) 1.5 nm, (c) 6 nm), as measured by AFM. Both the island and the cap-layer have been deposited at 750 °C.

In the uncapped sample (figure 11(a)), we can distinguish two different island families: the pyramids and the strained domes, with the latter being the vast majority of the island population. The average Ge content in islands deposited in the same conditions is $x = 0.55 \pm 0.05$ as measured by EXAFS [16], a value slightly higher than that reported in figure 8 (this discrepancy is explained in [16]).

The deposition of a silicon cap layer does not result in a immediate burial of the Ge islands. As a matter of fact, at first the supplied silicon atoms mainly enter and alloy into the existing islands, driving a morphological evolution of the Ge(Si) islands following a reverse Stranski–Krastanov dynamics [15, 16].

For a Si coverage $\theta_{Si} = 1.5$ nm, the strained domes undergo a morphological transition toward pyramids, as clearly visible in figure 11(b): most of the islands here are pyramids or elongated pyramids, with sides oriented along the [100] equivalent directions. This evolution is characterized by an increase of the island average base and, consequently, by an increase of the surface covered by islands, and by a decrease of the island aspect ratio down to $\alpha = 0.1$ [16], as expected for {105} pyramids. The morphological evolution is accompanied by a silicon enrichment of the island resulting in an average Ge content $x = 0.40 \pm 0.05$. A subsequent Si deposition entails a further enlargement of the islands and a further flattening of the islands (figure 11(c)). At this stage the islands have an average Ge content of about $x = 0.30$ and their shape is very close to the mesa-like shape observed by means of cross-sectional transmission electron microscopy (XTEM) in figure 7 in the buried layers.

We point out that the island density in this sample is equal, within the statistical error, to the density of the strained domes in the un-capped sample. Therefore, the strained pyramids present on the sample surface before the silicon cap-layer deposition have been dissolved and/or incorporated in larger islands as the capping proceeds.

The measured average volume of the islands remains almost constant as a function of the Si coverage. This can be explained taking into account the concurrent Si growth in the wetting layer region [16].

A further silicon deposition results in the burial of the islands and in the formation of a *real* capping layer, with the island composition remaining constant.

A striking feature of figures 11(a)–(c) is the increase of the island lateral ordering as the island enlargement proceeds. The ordering of the islands in a square super-lattice oriented along the elastically softer [100] and [010] direction is particularly evident in figure 11(c). To quantify such tendency towards enhanced ordering, in figure 11 we also display the histograms obtained calculating for each sample, on an area of about 100 μm^2, the angle θ_{NN} existing between the segment connecting the centre of each island to those of its four nearest neighbours and the crystallographic direction [110], used as a reference.

The homogeneous θ_{NN} distribution of figure 11(e) reflects the random island arrangement in the un-capped sample. In contrast, the θ_{NN} distributions of the two capped samples displayed in figures 11(f)–(g) present two peaks centred around $\pm 45°$, i.e. at the angles expected for islands disposed on a simple square lattice oriented along the [100] and [010] directions. The height and sharpness of the two peaks is strongly increased in the 6 nm thick cap layer samples in which the edges of adjacent islands closely approach each other, suggesting that the ordering is driven by island–island interaction.

7. Interpretation of the in-plane ordering: from elastic repulsion to lateral motion

From the experimental data presented in section 6 it is quite evident that, by partially capping the first layer of Ge islands with Si, enhanced lateral ordering is obtained. Since it is hard to conceive that islands with a base larger than $\sim$100 nm dissolve to reappear in a different position, we believe that the ordering process is triggered by lateral motion of the islands. Let us investigate the possible microscopic origin of such motion.

It is well known that Ge islands produce a compressive strain field in the WL and in the Si substrate, located around the regions where the base is sealed to the WL (see, e.g., [18, 42]). In the presence of two neighbouring islands, the compression caused by one island can directly influence the other one. As first suggested by the experimental results of Floro et al [43], short island–island distance can induce a significant repulsion, eventually leading to ordering. Here we shall try to get more insights on the physics of two close-by Ge islands and on the role played by Si partial capping, using MD simulations based on the Tersoff potential [32] and continuum elastic-theory calculations.

As explained in [44], we have considered a simplified geometry where actual square-base pyramidal islands are modelled as ridges bounded by {105} facets, infinitely extending along the [010] (y) direction. A schematic, cross-sectional representation of the simulation cell is shown in figure 12. The use of the ridge geometry allowed us to reduce the simulation-cell size along y by exploiting PBC which were applied in the plane parallel to the surface, exactly as in the calculations described in section 4. While substituting square-basis islands with ridges does not allow one to consider corner effects, the experimental orientation of the islands after capping (with roughly parallel bases, see section 6) suggests that our approximation should be sufficient to get the most important contributions of the strain field.

Two such ridges were placed at a distance d along the [100] direction, and simulations were run for different values of d, in order to explore the effect of the distant-dependent elastic

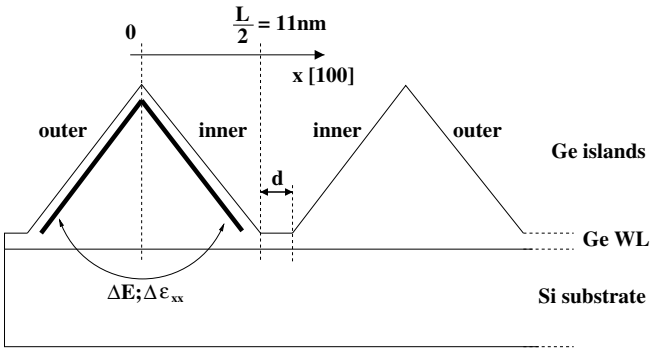

Figure 12. Cross-section of the geometry considered in the MD simulations. The aspect ratio of the islands has been magnified for a better representation. The use of PBC determines a ridge geometry, infinitely extending along the [010] direction (perpendicular to the image plane). In the calculations, the atoms close to the surface, but not exactly at the surface (see footnote 4), are selected. The position occupied by such atoms is schematized by a thick line inside the left island.

interaction. The base of the islands was set to $s = 22$ nm (corresponding to a height of 2.2 nm), while the substrate was made of a 3 ML thick Ge WL over a 5.4 nm thick Si substrate. As in the case treated in section 4, we shall rely on self-similarity, and compare simulated systems with all relevant dimensions roughly corresponding to $1/10$ of the experimental ones.

In order to avoid artificial lateral interactions caused by PBC in a significant range of d values, we considered a cell extending widely (74 nm) in the [100] (x) direction. The various structures which we have considered were optimized by a standard quenched-MD algorithm. After computing the strain tensor as in section 4, we obtained detailed information on both the the deformation field and the energy for each individual atom composing the system. Among these data, we focused our attention on the atoms residing in the close proximity of the free facets' surfaces[4]. In fact, at the typical experimental temperatures of interest, bulk diffusion is totally suppressed, so that only surface atoms (or atoms close enough to the free surfaces) can be held responsible for the observed lateral motion.

We shall start by analysing the case of two pure Ge ridges at a distance $d = 1$ nm. The ϵ_{xx} component of the strain field, which we verified to be the largest and the most sensitive to the presence of a close-by island, is plotted in figure 13(a). The values of ϵ_{xx} were obtained by averaging over the surface atoms selected as explained in footnote 4, and whose position is sketched in figure 12. Since two islands are present, the two facets of each of our ridges are not equivalent. Each ridge will be characterized by an *inner* facet, directly in front of the inner facet of the other island, and by an *outer* one, facing the flat WL, as emphasized in figure 12. Inner facets are naturally expected to feel the compressive field generated by the neighbouring island more strongly. This is clearly revealed by the results of figure 13(a) showing a pronounced asymmetry between inner and outer facet's atoms, both in terms of strain and of energy per atom. In the figure, $x = 0$ represents the coordinate of the ridge apex; the inner facet is characterized by $x \in (0, 11)$ nm, the outer by $x \in (-11, 0)$ nm. Obviously, in the absence of the other ridge, the energy and the strain at each position $x = \pm x_0$ would be exactly the same. Here, instead, both the energy and the strain *splitting* are strongly height dependent: close to the ridge base, the line connecting two opposite points at the same distance from the apex is

[4] We avoid considering atoms at the very surface, since their energy and strain would be strongly dependent on the atomistic details of possible reconstructions and/or on their coordination, which, during growth, could be strongly varying or unknown. Instead, we select atoms between 2 and 3 Å below the free surface.

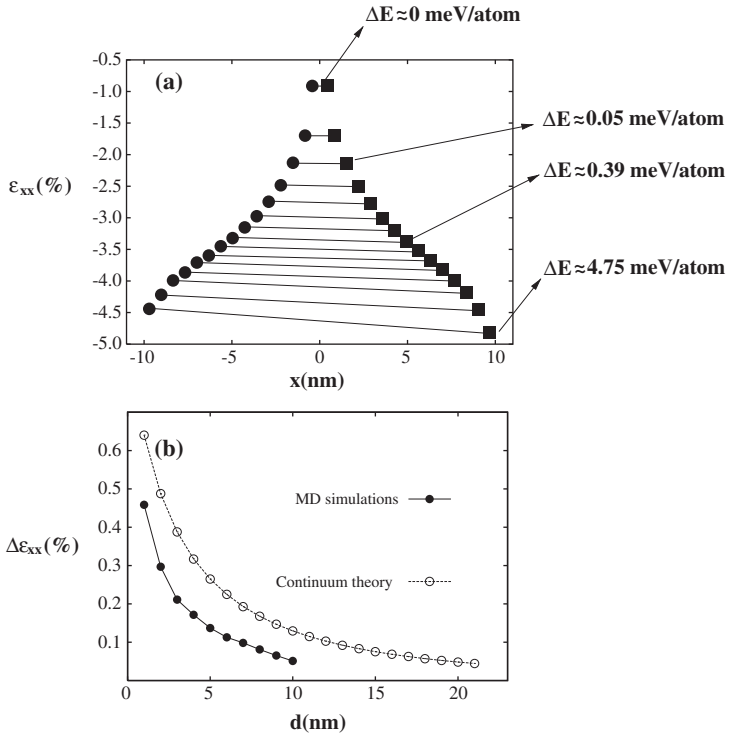

Figure 13. (a) Strain component ϵ_{xx} along the outer and inner facets of a Ge {105} ridge, in the presence of a neighbouring one placed at a distance $d = 1$ nm. The apex of the ridge is located at $x = 0$ nm. Filled circles represent outer-facet surface atoms, while filled squares are used for inner-facet surface atoms. For a few representative x positions, the corresponding energy per atom as computed by MD simulations is also given. (b) Difference in strain at the base of the ridge between inner and outer facets, as a function of the distance d to the neighbouring island. Filled circles represent MD simulations, while empty circles are the results of continuum elasticity theory calculations, in the framework of the flat-island approximation. MD results were computed only up to $d \sim 10$ nm, since for larger distance values spurious lateral interactions due to PBC start influencing the calculations.

very tilted. The corresponding average difference in energy is ∼4.75 meV/atom. By moving towards the apex, instead, inner and outer facets display a much more similar behaviour. In other words, the compressive field generated by one island is able to propagate along the inner facet of the other island only up to moderate heights (say, less than half of the total one). It is also interesting to note that the outer facet, instead, is almost insensitive to the presence of the other island (calculations for an isolated island yielded results hardly distinguishable from those of the outer facet reported in figure 13(a)). So, if two pure-Ge islands lie in close proximity, the surface Ge atoms of the two inner facets are strongly destabilized by the compressive field, finding lower-energy sites on the opposite sides. By increasing d, the above mentioned effect decreases in intensity, as shown in figure 13(b).

The results displayed in figure 13 were obtained under the assumption of non-intermixed islands, while the experiments revealed a very high concentration of Si after the inverse shape transformation (see section 6). While a more realistic attempt, based on continuum elasticity theory, to model the role of intermixing in influencing the strain field will be reported below, as a first step we have locally changed the composition of our ridges in the MD simulations

by (a) changing the type of the surface atoms at the base of the islands from Ge to Si and (b) transforming the four more external ridge layers from pure Ge to an ordered SiGe alloy. In both cases, the qualitative observation of a driving force pushing atoms from inner to upper facets was also confirmed for Si atoms. At the base of the island (i.e. precisely where intermixed Si is expected to be mainly present [45]), in case (a) we found an average energy splitting for Si atoms of the order of ∼2 meV/atom, reducing to ∼1.5 meV/atom in case (b). In other words, due to the very strong compression felt at the base of the inner facet, both Ge and Si atoms tend to be destabilized. We can envision that surface atoms, due to the high experimental temperature used in the experiments of section 6, are able to leave their original location within one facet, and to explore the other side of the island. If the island is isolated, on average, each facet would conserve the same number of atoms. If, on the other hand, a neighbouring island raises the energy of the inner facets, a net average flux of atoms from internal to external regions would induce an effective lateral motion pushing the islands to move along opposite directions, until the elastic interaction becomes negligible or until a new neighbouring island is encountered during the motion, inducing an inverse driving force. Notice that the experimental observation of an alignment along the [100]–[010] directions, which are the *soft* ones and allow for shorter inter-island distance, reinforces the idea of an ordering driven by elastic-energy lowering.

Obviously, all of the detailed atomic-scale mechanisms allowing the above underlined process to occur still need to be investigated, and the reported values of energy differences should be regarded as indicative. Still, we would like to point out that the idea of fast diffusion allowing surface atoms to quickly sample both sides of the island is compatible with the typical values of the kinetic barriers reported in the literature for Si/Ge systems. Indeed, by assuming a standard Arrhenius form of the diffusion coefficient (with a standard common prefactor of 10^{13} s^{-1}), and by imposing that atomic displacements as large as the islands' base (∼200 nm) can occur at least 10^4 times (i.e. *fast*) within the typical timescale and temperature of the experiments (∼10^2 s) reported in section 6, we obtain an upper bound of ∼1.04 eV for the maximum barrier, allowing atoms to move fast from one side to the other of the island. This estimate is much larger than the values reported in the literature for Si/Ge atom hopping (see, e.g., [46] and references therein), including diffusion along {105} facets [13]. Also, it is fully compatible with reported Si_2 and Ge_2 diffusion barriers [47].

In the experiments discussed in section 6, the evidence for lateral motion of the islands was reported only after Si partial capping, and could be inferred thanks to the enhanced degree of ordering. It is thus fundamental to explore further the role of Si. If from one side capping produces a decrease in the average distance between islands' edges (thus enhancing inner versus outer facet energy splitting), a clear reduction of the average aspect ratio and an increase in the Si content is also observed. Since the latter phenomenon leads to a reduction of the compressive field, it seems to be key to take into account at the same time shape, average distance, and composition, in order to understand the actual evolution of the compressive field during capping. To investigate this issue, we have used continuum elasticity theory, since a detailed atomistic investigation of the role played by changes in shape and in composition is particularly demanding from the computational point of view (the possibility to build up a model of Si intermixing in Ge islands using an atomistic approach and a Monte Carlo scheme can be found in [48–50]). A particularly suitable approach exploits the knowledge of the analytical expression for the Green tensor $G_{i,j}$ of a semi-infinite isotropic elastic body [28], which gives the deformation field induced in the body by a point-like force acting at its surface (located at $z = 0$) through the relation

$$u_i(x, y, z = 0) = G_{ik}(x, y, z = 0)F_k. \tag{4}$$

In equation (4), u_i is the ith component of the displacement field, while F_k is the kth component of a concentrated force: $F_k\delta(x)\delta(y) = P_k(x, y)$; P representing the force density at the surface. Since G_{ik} is known (see [28] for the complete form), one can compute the displacement field due to a generic force density by integration:

$$u_i(x, y, z = 0) = \int\int G_{ik}(x - x', y - y', z = 0)\, P_k(x', y')\, \mathrm{d}x'\, \mathrm{d}y'. \tag{5}$$

In the so-called *flat-island approximation* [51] the deformation field induced by a Ge ridge (i.e. by an island infinitely extending along the y direction, as in our MD calculations) on Si is described by the following simple expression for the surface force density:

$$P_x(x) = \bar{\sigma}\frac{\partial h(x)}{\partial x}, \tag{6}$$

where $\bar{\sigma}$ corresponds to the constant σ_{xx} component for a Ge layer uniformly compressed at 4.2%. By inserting equation (6) into (5), after some calculations [52, 53] one obtains the following expression for the $\epsilon_{xx}(x)$ component of the strain field induced by the island at any x position:

$$\epsilon_{xx} = \epsilon_0 + 2\frac{1+\nu}{\pi}\epsilon_0 \tan\theta \log\left|\frac{(x - H\cot\theta)(x + H\cot\theta - L)}{x(x - L)}\right|. \tag{7}$$

In equation (7), L is the base length, θ the inclination angle of the island facets, ν the material Poisson ratio, ϵ_0 the misfit strain (4.2%), and H the island height.

In the presence of two islands separated by d, the total strain field can be computed by summing each individual contribution given by equation (7). When analysing the results of the MD simulations, we have pointed out that the island–island interaction induces a difference $\Delta\epsilon_{xx}$ between the strain in the inner and outer facets (see figure 13), which is particularly strong in the proximity of the base of the facet. Let us then analyse $\Delta\epsilon_{xx}$ (computed exactly at the x positions corresponding to the stronger compression in figure 13(a) as predicted by equation (7)). Despite its simple form and the reduced dimensionality, equation (7) yields results in qualitative agreement [44] with MD simulations. For example, a direct comparison between $\Delta\epsilon_{xx}$ as computed by MD and from equation (7) for different values of the island–island distance d is reported in figure 13(b), for the case of pure-Ge ridges considered in the MD simulations. The trend is clearly the same, and the values are reasonably close. Still, a tendency of the continuum theory to overestimate the interaction effect can be spotted. A detailed comparison between atomistic results and the flat-island approximation for different aspect-ratio values is reported in [54], where the effect of neglecting the base-to-apex lattice-parameter relaxation while deriving equation (7) is critically analysed.

After validating the continuum approach, we can finally use it to compare the typical configurations encountered during the inverse-shape transition induced by partial capping discussed in section 6. As schematized in figure 14, we have first considered two high aspect-ratio (0.2) islands, at a given distance. Then, we have kept their volume and centre-of-mass position fixed (the apex–apex distance being set to $\sim 2.25L$, as suggested by the experimental data of figure 11), and allowed for a change in shape leading to 0.1 (panel (b)) and 0.05 (panel (c)) aspect-ratio islands. The change in $\Delta\epsilon_{xx}$ along this transformation, computed by using equation (7) is shown in figure 14(d) by filled circles. It appears rather clearly that, in spite of the reduction of the aspect ratio, the decreased distance between the island edges induces a stronger difference in strain (and, thus, in energy) from inner to outer facet, favouring a lateral motion able to increase the island–island distance. Finally, we have also tried to model the differences in composition which take place during the shape transformation by replacing ϵ_0 in equation (7) with the effective average mismatch in a SiGe island of a given Ge composition.

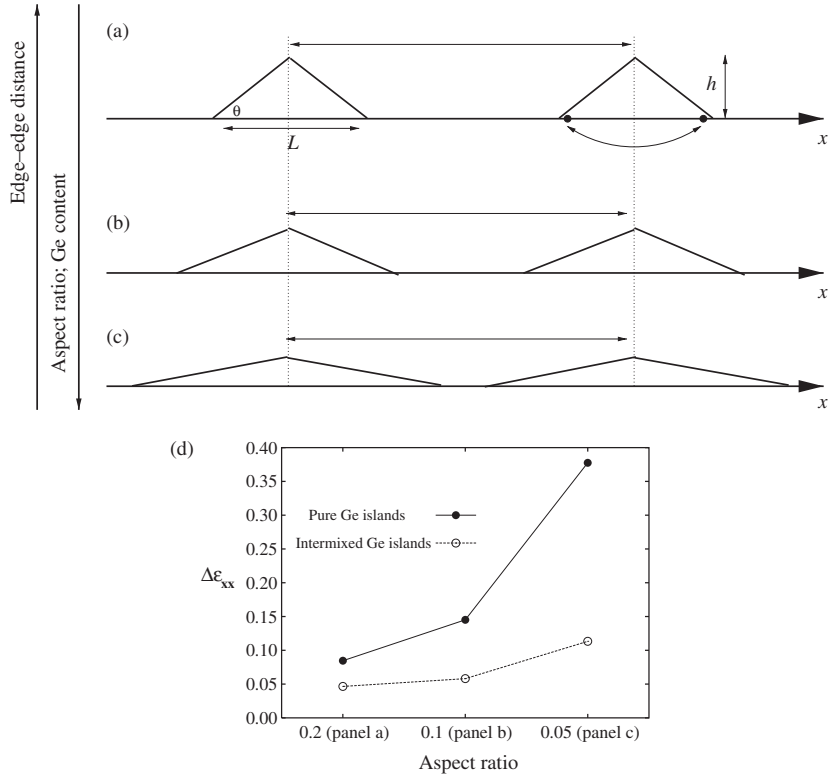

Figure 14. (a)–(c) Different geometries considered in our continuum-theory calculations. Panel (a) corresponds to a 0.2 aspect ratio, panel (b) to 0.1 and panel (c) to 0.05, in an attempt to model the experimental CVD data (section 6). The triangles representing the islands are drawn with double aspect ratio with respect to the actual ones, for a better representation. (d) $\Delta\epsilon_{xx}$ computed for the configurations illustrated in panels (a)–(c) for pure-Ge islands (filled circles) and for intermixed islands (empty circles) with a Ge concentration $c_{\mathrm{Ge}} = 0.55$, 0.40, and 0.3 for the 0.2, 0.1, and 0.05 aspect-ratio islands, respectively.

Also considering that flatter islands are more intermixed, the trend still remains the same (see empty circles in figure 14(d)), even if the $\Delta\epsilon_{xx}$ values become smaller.

Summarizing, we have first shown by accurate MD simulations that the elastic interaction between neighbouring Ge islands deeply influences (at short distances) the atoms close to the facets' free surfaces. Inner facets are more compressed and bonds are weaker, so that a transfer of atoms from inner to outer facets is thermodynamically favoured, especially in the region closer to the base. If an inverse shape transformation roughly conserving the volume takes place, the difference in strain field between inner and outer facets grows, in spite of the lower island aspect ratio and of the higher Si concentration. In this sense, Si partial capping helps promoting lateral motion. Notice that in this context the difference in energy per atom between inner and outer facets plays the same role of the position-dependent chemical potential introduced in section 4 to explain vertical ordering.

To further prove that our general picture has predictive power, a new set of experimental samples was grown by trying to enhance two of the main driving forces for ordering. While the same procedure described in section 6 was used, the amount of deposited Ge was raised to 3 nm of equivalent thickness, while the growth temperature was lowered to 600 °C. In this way,

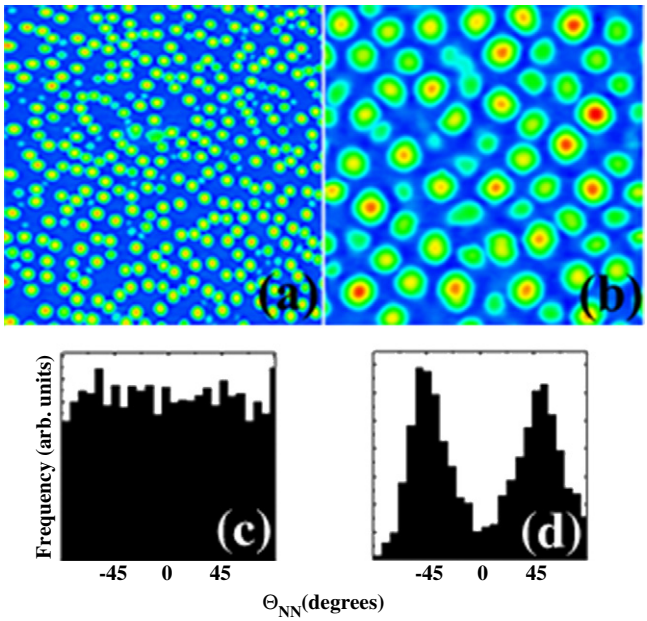

Figure 15. $2 \times 2\ \mu m^2$ AFM images of samples grown by depositing 3 nm of Ge equivalent thickness at 600 °C. (a) As-grown sample. (b) After 6 nm Si capping at 750 °C. The corresponding first-neighbour angular distributions are shown in panels (c) and (d). The figure is reprinted with permission from [44]. Copyright 2006, American Physical Society.

we have produced a higher island density (compare figure 11(a) with figure 15(a)), with a lower degree of intermixing (see section 7). After capping, the degree of ordering is clearly enhanced with respect to the previously discussed results (compare figure 11(f) with figure 15(d)) because of the repulsive effect due to the very short edge–edge distances and by the less pronounced intermixing-induced relaxation of the strain field.

8. Direct evidence for large Ge island lateral motion

Although we believe our interpretation of a lateral motion producing enhanced ordering to be rather convincing, we cannot claim to have observed such motion directly. While we were gathering the final data shown in section 6 and refining their theoretical interpretation, a paper presenting closely related results appeared in the literature [55]. Although no changes in lateral ordering were reported, large (intermixed) Ge islands on Si(001) were shown to display lateral motion, triggered by post-growth annealing. While even in [55] islands were not directly observed to move (i.e. by a real-time *in situ* STM movie), their displacements were inferred from the *footprints* left on the substrate by their presence, revealed after island removal by an etching procedure. This technique seems solid and it has been shown to yield very valuable information on the past history of an island [56–58]. Island gliding was first interpreted by the authors of [55] as caused by a surface-mediated alloying process. In practice, a fluctuation of Si content between two opposite sides of the island would promote a flux of Ge atoms from the less intermixed to the opposite side, the driving force being originated by both alloying-induced strain relaxation and by a purely entropic term. At temperatures high enough to guarantee continuous Si supply from the substrate, the above described process is

self-sustained, and islands can migrate (while enlarging their volume) until the Si concentration is too high to induce further advantages in moving Ge atoms from one side to the other. In the original work, the initial fluctuation in Si content appeared to be random, so that such a kind of motion could not be exploited to achieve enhanced lateral ordering. The proposed mechanism is surely intriguing and could be complementary to the one here proposed even if, under certain circumstances, the role of the elastic repulsion seems to be key. While the presence of additional Si in our partial-capping experiments could strongly help in promoting alloying, on the other hand the typical concentration of Si (∼70%, see section 6) in the ordered islands is so high that it is hard to conceive a further driving force for intermixing. Also, in a more recent paper [58], Stoffel *et al* observed a clear directionality of the lateral motion, with neighbouring islands moving along opposite directions. An explanation of the results very close to ours was given. Still, both the alloying-induced lowering of the strain field and the entropic contribution are expected to be present in a real system. Further theoretical work dedicated to quantitatively characterizing both surface-mediated alloying and repulsive effects is surely needed in order to build a fully predictive model of island lateral motion.

9. Conclusions

In this work we have presented a set of results obtained in the last few years by our research groups in a combined theoretical and experimental effort aimed at building a unified view of some key processes occurring when Ge islands form on Si. One of the main features of such systems is that at the typical temperatures of interest bulk diffusion is totally frozen while surface diffusion is fast. This allows one to look at several phenomena by simple local thermodynamics: if atoms in the close proximity of a free surface have the possibility to migrate in a lower-energy region (still close to a free surface) they are assumed to do so. To this end, an accurate mapping of local differences in the atomic chemical potential at the surface is a crucial quantity to be estimated. While knowing that this *modus operandi* is not expected to work in general, and that direct evaluation of kinetic parameters at the atomic scale is often needed, here we have offered a few examples where it did work, leading to a nice agreement between theory and experiments. If for the study of vertical ordering simulations and AFM images agreed also from a quantitative point of view, a more qualitative, although rather consistent, theoretical picture of partial-Si-capping induced lateral ordering has been given.

Acknowledgments

We would like to thank P Raiteri, R Marchetti, S Cereda, V A Zinovyev, G Vastola, C Spinella and F Evangelisti for their contributions to the original work which originated the present review.

FM, AM, and LM acknowledge financial support under the European Union project d-DOT-FET (contract number 012150).

References

[1] Cullis A G and Booker G R 1971 *J. Cryst. Growth* **9** 132
[2] Aleksandrov L N, Lovyagiv R N, Pchelyakov O P and Stenin S I 1974 *J. Cryst. Growth* **24/25** 298
[3] Eaglesham D J and Cerullo M 1990 *Phys. Rev. Lett.* **64** 1943
[4] Mo Y-W, Savage D E, Swartzentruber B S and Lagally M G 1990 *Phys. Rev. Lett.* **65** 1020
[5] Capellini G, Di Gaspare L, Evangelisti F and Palange E 1997 *Appl. Phys. Lett.* **70** 493
[6] Medeiros-Ribeiro G, Bratkovski A M, Kamins T I, Ohlberg D A A and Williams R S 1998 *Science* **279** 353
[7] Ross F M, Tromp R M and Reuter M C 1999 *Science* **286** 1931
[8] Daruka I, Tersoff J and Barabasi A-L 1999 *Phys. Rev. Lett.* **82** 2753

[9] Daruka I and Tersoff J 2002 *Phys. Rev.* B **66** 132104
[10] Montalenti F, Raiteri P, Migas D B, von Känel H, Rastelli A, Manzano C, Costantini G, Denker U, Schmidt O G, Kern K and Miglio L 2004 *Phys. Rev. Lett.* **93** 216102
[11] Zela V, Pietzonka I, Sass T, Thelander C, Jeppesen S and Seifert W 2002 *Physica* E **13** 1013
[12] Johansson J and Seifert W 2002 *J. Cryst. Growth* **234** 139
[13] Montalenti F, Migas D B, Gamba F and Miglio L 2004 *Phys. Rev.* B **70** 245315
[14] Cereda S, Montalenti F and Miglio L 2005 *Surf. Sci.* **591** 23
[15] Rastelli A, Kummer M and von Känel H 2001 *Phys. Rev. Lett.* **87** 256101
[16] Capellini G, De Seta M, Di Gaspare L, Evangelisti F and d'Acapito F 2005 *J. Appl. Phys.* **98** 124901
[17] Tersoff J, Teichert C and Lagally M G 1996 *Phys. Rev. Lett.* **76** 1675
[18] Shchukin V A and Bimberg D 1999 *Rev. Mod. Phys.* **71** 1125
[19] Voigtländer B 2001 *Surf. Sci. Rep.* **43** 127
[20] Brunner K 2002 *Rep. Prog. Phys.* **65** 27
[21] Pchelyakov O P, Bolkhovityanov Yu B, Dvurechenskii A V, Sokolov L V, Nikiforov A I, Yakimov A I and Voigtländer B 2002 *Semiconductors* **34** 1229
[22] Stangl J, Holy V and Bauer G 2004 *Rev. Mod. Phys.* **76** 725
[23] Barth J B, Costantini G and Kern K 2005 *Nature* **437** 671
[24] Baribeau J-M, Wu X, Rowell N L and Lockwood D J 2006 *J. Phys.: Condens. Matter* **18** R139
[25] Maradudin A A and Wallis R F 1980 *Surf. Sci.* **91** 423
[26] Zhong J, Wells J C, Niu Q and Zhang Z 2003 *Surf. Sci.* **539** L525
[27] Zhang J, Zhang K and Zhong J 2004 *Appl. Phys. Lett.* **84** 1853
[28] Landau L D and Lifshitz E M 1986 *Theory of Elasticity-Course of Theoretical Physics* vol 7 (Oxford: Butterworth-Heinemann)
[29] Phillips R 2001 *Crystals, Defects, and Microstructures* (Cambridge: Cambridge University Press)
[30] Makeev M A and Madhukar A 2001 *Phys. Rev. Lett.* **86** 5542
[31] Marzegalli A, Montalenti F and Miglio L 2005 *J. Phys.: Condens. Matter* **17** 7505
[32] Tersoff J 1989 *Phys. Rev.* B **39** 5566
[33] Migas D B, Cereda S, Montalenti F and Miglio L 2004 *Surf. Sci.* **556** 121
[34] Smith A P, Wiggs J K, Jónsson H, Yan H, Corrales J, Nachtigali P and Jordan K D 1995 *J. Chem. Phys.* **102** 1044
[35] Capellini G, De Seta M, Spinella C and Evangelisti F 2003 *Appl. Phys. Lett.* **82** 1772
[36] Marchetti R, Montalenti F, Miglio L, Capellini G, De Seta M and Evangelisti F 2005 *Appl. Phys. Lett.* **87** 261919
[37] Raiteri P 2002 *PhD Thesis* Univerità degli Studi di Milano Bicocca
[38] Pryor C, Kim J, Wang L W, Williamson A J and Zunger A 1998 *J. Appl. Phys.* **83** 2548
[39] De Seta M, Capellini G and Evangelisti F 2005 *Phys. Rev.* B **71** 115308
[40] De Seta M, Capellini G, Evangelisti F and Spinella C 2002 *J. Appl. Phys.* **92** 614
[41] Capellini G, De Seta M and Evangelisti F 2001 *Appl. Phys. Lett.* **78** 303
[42] Raiteri P, Miglio L, Valentinotti F and Celino M 2002 *Appl. Phys. Lett.* **80** 3736
[43] Floro J A, Chason E, Sinclair M B, Freund L B and Lucadamo G A 1998 *Appl. Phys. Lett.* **73** 951
[44] Capellini G, De Seta M, Evangelisti F, Zinovyev V A, Vastola G, Montalenti F and Miglio L 2006 *Phys. Rev. Lett.* **96** 106102
[45] Magalhaes-Paniago R, Medeiros-Ribeiro G, Malachias A, Kycia S, Kamins T I and Stan Williams R 2002 *Phys. Rev.* B **66** 245312
[46] van de Walle A, Asta M and Voorhes P W 2003 *Phys. Rev.* B **67** 041308(R)
[47] Lu Z-Y, Wang C-Z and Ho K-M 2000 *Phys. Rev.* B **62** 8104
[48] Sonnet Ph and Kelires P C 2002 *Phys. Rev.* B **66** 205307
[49] Kelires P C 2004 *J. Phys.: Condens. Matter* **16** S1485
[50] Hadjisavvas G and Kelires P C 2005 *Phys. Rev.* B **72** 075334
[51] Tersoff J and Tromp R M 1993 *Phys. Rev. Lett.* **70** 2782
[52] Penev E 2002 *PhD Thesis* Technischen Universität Berlin
[53] Kratzer P, Penev E and Scheffler M 2002 *Appl. Phys.* A **75** 79
[54] Zinovyev V A, Vastola G, Montalenti F and Miglio L 2006 in preparation
[55] Denker U, Rastelli A, Stoffel M, Tersoff J, Katsaros G, Costantini G, Kern K, Jin-Phillipp N Y, Jesson D E and Schmidt O G 2005 *Phys. Rev. Lett.* **94** 216103
[56] Katsaros G, Costantini G, Stoffel M, Esteban R, Bittner A M, Rastelli A, Denker U, Schmidt O G and Kern K 2005 *Phys. Rev.* B **72** 195320
[57] Rastelli A, Stoffel M, Tersoff J, Kar G S and Schmidt O G 2005 *Phys. Rev. Lett.* **95** 026103
[58] Stoffel M, Rastelli A, Kiravittaya S and Schmidt O G 2005 *Phys. Rev.* B **72** 205411